AIP Journal of Applied Physics

Thermal stability of Ba (Zr 0.8 − x Ce x Y 0.2) O 2.9 ceramics in carbon dioxide

C.-S. Tu, R. R. Chien, V. H. Schmidt, S.-C. Lee, C.-C. Huang, and C.-L. Tsai

Citation: Journal of Applied Physics **105**, 103504 (2009); doi: 10.1063/1.3117835
View online: http://dx.doi.org/10.1063/1.3117835
View Table of Contents: http://scitation.aip.org/content/aip/journal/jap/105/10?ver=pdfcov
Published by the AIP Publishing

Thermal stability of $Ba(Zr_{0.8-x}Ce_xY_{0.2})O_{2.9}$ ceramics in carbon dioxide

C.-S. Tu,[1,2,a] R. R. Chien,[3] V. H. Schmidt,[3] S.-C. Lee,[2] C.-C. Huang,[2] and C.-L. Tsai[3]
[1]*Graduate Institute of Applied Science and Engineering, Fu Jen Catholic University, Taipei, Taiwan 242, Republic of China*
[2]*Department of Physics, Fu Jen Catholic University, Taipei, Taiwan 242, Republic of China*
[3]*Department of Physics, Montana State University, Bozeman, Montana 59717, USA*

(Received 11 October 2008; accepted 18 March 2009; published online 18 May 2009)

In situ x-ray diffraction spectra (25–1000 °C) have been measured as a function of temperature for proton-conducting $Ba(Zr_{0.8-x}Ce_xY_{0.2})O_{2.9}$ ($x=0.0-0.4$) ceramics in CO_2 atmosphere. Atomic vibrations before and after exposure to CO_2 were obtained by using the micro-Raman scattering (150–1600 cm^{-1}). $Ba(Zr_{0.8}Y_{0.2})O_{2.9}$ and $Ba(Zr_{0.6}Ce_{0.2}Y_{0.2})O_{2.9}$ reveal a promising thermal stability in CO_2 without apparent decomposition up to 1000 °C. However, $Ba(Zr_{0.5}Ce_{0.3}Y_{0.2})O_{2.9}$ and $Ba(Zr_{0.4}Ce_{0.4}Y_{0.2})O_{2.9}$ exhibit thermally stable below 550 °C and then proceed an obvious chemical decomposition of $BaCO_3$ and $Zr_{0.8-x}Ce_xY_{0.2}O_2$ above 550 °C, which were clearly evidenced by the Raman vibrations of 1057 and 466 cm^{-1}, respectively. A first-order orthorhombic-hexagonal structure transition was confirmed in $BaCO_3$ in the region of 810–850 °C upon heating. This study suggests that the $Ba(Zr_{0.8-x}Ce_xY_{0.2})O_{2.9}$ ceramics with $x \leq 0.2$ are promising candidates for proton-conducting applications in CO_2-containing environment. © *2009 American Institute of Physics*. [DOI: 10.1063/1.3117835]

I. INTRODUCTION

One challenging issue in proton-conducting ceramics for applications of hydrogen purification and solid oxide fuel cell (SOFC) electrolytes is thermal instability due to the reaction with environment, especially components of hydrocarbon fuels such as CO_2, H_2S, and other trace species.[1–3] Such unfavorable reactions with carbon species and H_2S could cause performance loss and degradation. However, the effect of species of hydrocarbon fuels on SOFC materials is not presently well known. Although proton conductors are promising candidates for SOFC at intermediate temperatures (typically 700–850 °C) because of their low activation energy,[4–7] the remained challenge is to find an appropriate compromise between ionic conductivity and thermal stability in various environments.

Doped $BaCeO_3$ has been known to exhibit high ionic conductivity above 500 °C and poor stability in CO_2 and H_2O.[4–13] On the other hand, yttrium-doped $BaZrO_3$ shows a sufficient thermal stability.[14,15] Partially substituting Zr for Ce can reduce tendency of decomposition in CO_2 at high temperature but decreases the ionic conductivity. Therefore, it has been a goal to find doped $Ba(Zr,Ce)O_3$ ceramics with sufficient ionic conductivity and thermal stability by replacing a fraction of cerium with Zr or other dopants.[14–22]

By thermal gravimetric analysis (TGA) and x-ray diffraction (XRD), $BaCe_{0.9}Y_{0.1}O_{3-\delta}$ (BCY10) powder was confirmed to be only kinetically stable below 500 °C and then decomposes completely to $BaCO_3$, CeO_2, and Y_2O_3 after heating in pure CO_2 at 860 °C.[8] Similarly, powder XRD result of BCY10 heated in 100% CO_2 in the range of 700–1000 °C evidenced $BaCO_3$ and fluoritelike CeO_2 structure.[9] It was found that BCY10 can absorb 0.13 g of CO_2 per ceramic gram.[9] $BaCe_{0.9}Nd_{0.1}O_{3-\delta}$ (BCN) ceramic also showed decomposition of $BaCO_3$ and CeO_2 in 1 atm CO_2 before reaching 1200 °C.[10] Above 1200 °C, the BCN ceramics reacted with alumina or zirconia, leading to the loss of barium and an excess of cerium.[10]

The XRD result of $BaZr_{0.4}Ce_{0.5}Y_{0.1}O_{3-\delta}$ showed a good stability after exposure to CO_2 at 900 °C.[12] The total conductivity of $BaZr_xCe_{0.9-x}Y_{0.1}O_{3-\delta}$ ($x=0.0-0.9$) in wet H_2 ($pH_2O=1.7\times10^3$ Pa) varies from 3.5×10^{-2} to 3.0×10^{-3} S cm^{-1} at 800 °C.[12] The XRD spectra of $Ba(Zr_{0.4}Ce_{0.5}Y_{0.1})O_{2.95}$ and $Ba(Zr_{0.6}Ce_{0.3}Y_{0.1})O_{2.95}$ sintered pellets showed good stability after being boiled in water or after being exposed to CO_2 at 900 °C.[13] TGA and differential thermal analysis of Gd- and Nd-doped $Ba(Ce,Zr)O_3$ solid solutions showed a reaction with CO_2 above 600 °C and a reverse reaction at about 1150 °C for low Zr content.[16]

Recent XRD investigation of $Ba(Ce_{0.8}Y_{0.2})O_3$ and $Ba(Zr_{0.1}Ce_{0.7}Y_{0.2})O_{3-\delta}$ powders exposed to 2% CO_2 (with H_2) at 500 °C for 1 week suggested that $Ba(Ce_{0.8}Y_{0.2})O_3$ decomposed to $BaCO_3$, CeO_2, and Y_2O_3.[18] However, $Ba(Zr_{0.1}Ce_{0.7}Y_{0.2})O_{3-\delta}$ remained unchanged at 500 °C and exhibited sufficient stability in 2% CO_2 atmosphere.[18] The XRD result of $Ba(Zr_{0.1}Ce_{0.7}Y_{0.2})O_{3-\delta}$ powder before and after exposure to H_2 containing 15% H_2O at 500 °C showed no decomposition.[18] Most recently, double perovskitelike $Ba_2(Ca_{0.75}Nb_{0.59}Ta_{0.66})O_{6-\delta}$, $Ba_2(Ca_{0.75}Nb_{0.66}Ta_{0.59})O_{6-\delta}$, and $Ba_2(Ca_{0.79}Nb_{0.66}Ta_{0.55})O_{6-\delta}$ showed a long-term structural stability in CO_2 at 800 °C and boiling water.[23]

Although proton-conducting ceramics are promising candidates for SOFC, the major issue for these materials is to find appropriate components with a wide-temperature-range thermal stability in various environments. In this work, *in situ* temperature-dependent XRD and post-micro-Raman scattering were employed to investigate the structure stability

[a]Author to whom correspondence should be addressed. Electronic mail: 039611@mail.fju.edu.tw.

of $Ba(Zr_{0.8-x}Ce_xY_{0.2})O_{2.9}$ (x=0.0, 0.2, 0.3, and 0.4) ceramic powders before and after exposure to CO_2 in the temperature region of 25–1000 °C.

II. EXPERIMENTAL PROCEDURE

$Ba(Zr_{0.8-x}Ce_xY_{0.2})O_{2.9}$ (x=0.0, 0.2, 0.3, and 0.4) ceramic powders were synthesized by the glycine-nitrate process.[24] Synthesized powders were calcined at 1300 °C for 5 h to optimize the perovskite phase. Hereafter, BZCY442, BZCY532, BZCY622, and BZY82 represent $Ba(Zr_{0.4}Ce_{0.4}Y_{0.2})O_{2.9}$, $Ba(Zr_{0.5}Ce_{0.3}Y_{0.2})O_{2.9}$, $Ba(Zr_{0.6}Ce_{0.2}Y_{0.2})O_{2.9}$, and $Ba(Zr_{0.8}Y_{0.2})O_{2.9}$, respectively. $Ba(Zr,Ce,Y)O_3$ and $(Zr,Ce,Y)O_2$ symbolize $Ba(Zr_{0.8-x}Ce_xY_{0.2})O_{2.9}$ and $Zr_{0.8-x}Ce_xY_{0.2}O_2$, respectively. For *in situ* XRD measurements, a Rigaku Model MultiFlex x-ray diffractometer with Cu $K\alpha_1$ and Cu $K\alpha_2$ radiations was used. The intensity ratio between $K\alpha_1$ and $K\alpha_2$ is about 2:1.[25] The calcined powders were scanned at room temperature first before flowing CO_2, and then the atmosphere was switched to flow at 1 atm CO_2. The temperature was raised in steps from room temperature. Each XRD scan was taken after holding the powder for more than 40 min at the setting temperature to allow complete reaction with CO_2.

A double grating Jobin Yvon Model U-1000 double monochromator with 1800 grooves/mm gratings and a nitrogen-cooled charge coupled device as a detector were employed for the post-micro-Raman scattering. A Coherent Model Innova 90 argon laser with wavelength λ =514.5 nm was used as an excitation source. The Raman scattering was performed in the region of 150–1600 cm^{-1}. The powder used in the post-Raman scattering measurements was previously exposed to CO_2 during the *in situ* XRD.

III. RESULTS AND DISCUSSION

To understand structure transition of $BaCO_3$, temperature-dependent XRD spectra of $BaCO_3$ powder were measured in 1 atm CO_2, as shown in Fig. 1(a). The strongest 2θ-peak appears at 24.0° at room temperature, indicating an orthorhombic phase.[25] Near 810 °C, two new peaks appear at 21.2° and 25.9°, suggesting a new phase. As temperature increases, the orthorhombic phase disappears completely near 850 °C. These phenomena reveal a first-order orthorhombic-hexagonal[26,27] structural transition in the region of 810–850 °C.

To identify possible decomposition, the XRD spectra of ZrO_2, CeO_2, and Y_2O_3 powders were obtained at room temperature as given in Fig. 1(b). The main 2θ peaks appear at 28.2° and 31.5° for monoclinic ZrO_2 and 28.5°, 33.0°, 47.5°, and 56.2° for cubic CeO_2. For cubic Y_2O_3, the main 2θ peaks occur at 29.2°, 33.9°, 48.5°, and 57.8°. There is no phase transformation for both ZrO_2 and CeO_2 below 1000 °C.[28,29] $BaCeO_3$ has a phase sequence of orthorhombic (*Pnma*)-orthorhombic (*Imma*)-rhombohedral ($R\bar{3}c$)-cubic ($Pm\bar{3}m$) at 290, 400, and 900 °C.[30] $BaZrO_3$ is cubic at and above room temperature.[31]

Figure 2(a) shows the XRD spectrum of BZCY442 powder before exposure to CO_2. The main 2θ peaks include (110), (200), (211), (220), (310), and (222) and suggest a body-centered cubic structure, but the weak (111) peak is consistent with the expected simple-cubic (sc) perovskite structure, according to a structure-factor calculation.[25] The (100) peak expected for sc is too weak to see in BZCY442 because the reflections from the (100) planes containing BaO are almost exactly cancelled by the reflections from the (100) planes containing $Zr_{0.4}Ce_{0.4}Y_{0.2}O_2$. The cubic lattice parameter was estimated from the strongest (110) peak to be a =4.322 Å. Two weak peaks as indicated by * near the (200) and (310) peaks correlate to a second phase.

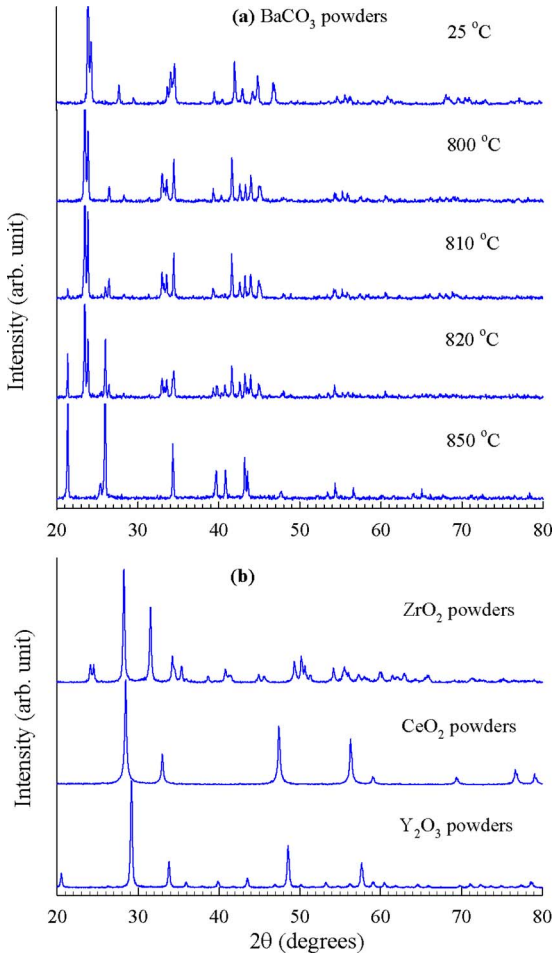

FIG. 1. (Color online) (a) *In situ* XRD spectra of $BaCO_3$ powder (99.9%) in 1 atm CO_2 and (b) XRD spectra of ZrO_2, CeO_2, and Y_2O_3 powders (99.9%) taken at room temperature.

As shown in Figs. 2(b)–2(e), the XRD spectra remain almost the same below 550 °C. At 600 °C the orthorhombic peak (2θ=23.7°) of $BaCO_3$ appears as denoted by "A." In addition, four weak broad peaks were observed at 28.5°, 33.5°, 47.9°, and 56.5° as indicated by "B." These weak broad peaks most likely correspond to a CeO_2-like structure because their XRD peaks close to main peaks of CeO_2 [Fig. 1(b)]. The intensities of A and B peaks grow gradually as temperature increases. At 900 °C [Fig. 2(j)] A peak disappears and two new peaks appear at 21.4° and 25.9° as indicated by "C," confirming an orthorhombic-hexagonal transformation of $BaCO_3$.

Figures 3(a)–3(d) show Raman spectra of ZrO_2, CeO_2, Y_2O_3, and $BaCO_3$ powders taken at room temperature. The major vibrations are 474, 461, and 375 cm^{-1} for ZrO_2,

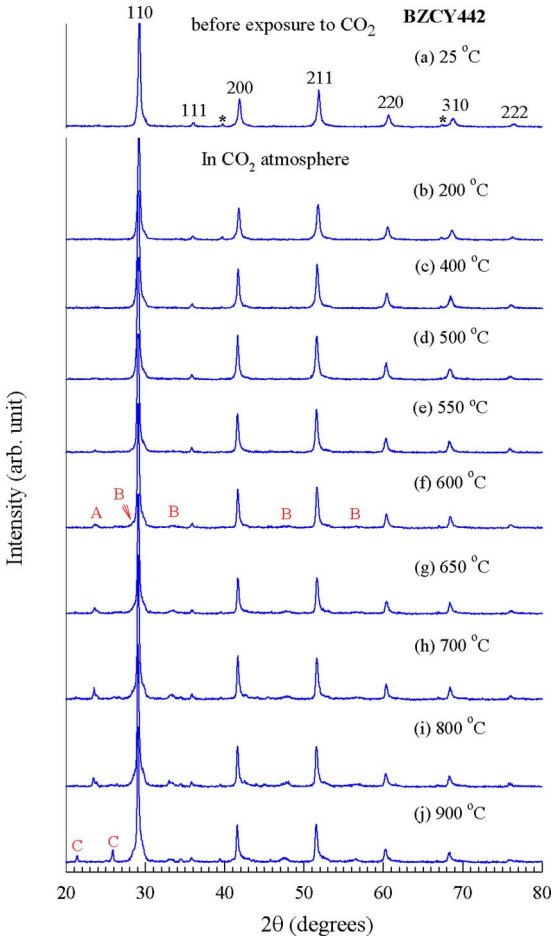

FIG. 2. (Color online) Temperature-dependent XRD spectra of BZCY442. A, B, and C peaks correspond to orthorhombic $BaCO_3$, cubic $(Zr,Ce,Y)O_2$, and hexagonal $BaCO_3$, respectively.

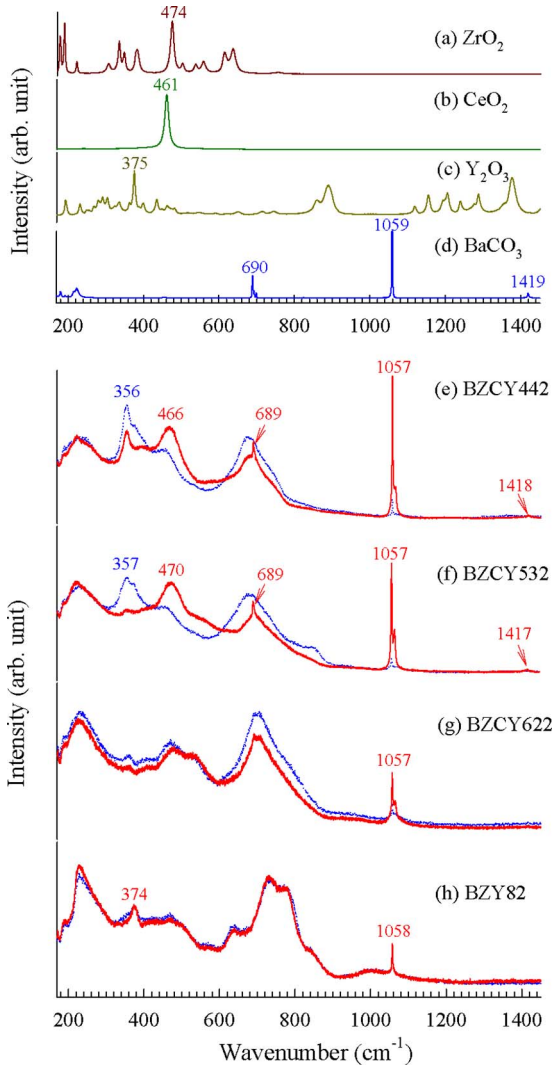

FIG. 3. (Color online) (Color online) Raman spectra of (a) ZrO_2, (b) CeO_2, (c) Y_2O_3, (d) $BaCO_3$, (e) BZCY442, (f) BZCY532, (g) BZCY622, and (h) BZY82 powders measured at room temperature. Blue dotted lines are spectra taken before exposure to CO_2. Red solid lines are spectra taken after exposure to CO_2.

CeO_2, and Y_2O_3, respectively. The 474 cm^{-1} of ZrO_2 corresponds to the A_g Raman-active mode of O–O vibration.[32] The 461 cm^{-1} vibration of CeO_2 results from the F_{2g} Raman-active mode of fluorite structure.[33] The main vibrations of $BaCO_3$ include 690, 1059, and 1419 cm^{-1} [Fig. 3(d)], which correspond respectively to the doubly degenerate bending mode (E''), symmetric stretching vibration (A_1'), and doubly degenerate asymmetric stretching vibration (E') of CO_3^{2-} ion.[34] The chemical decompositions occurred in BZCY442 were confirmed by 689, 1057, and 1418 cm^{-1} for $BaCO_3$ and 466 cm^{-1} for $(Zr,Ce,Y)O_2$ [Fig. 3(e)]. Note that the 466 cm^{-1} is between 461 cm^{-1} of CeO_2 and 474 cm^{-1} of ZrO_2, but there are no peaks corresponding to the other ZrO_2 peaks. Another evidence for cubic fluorite structure is that the major Raman vibrations of both Zr–Ce–O (Ce/Zr =1) and Si-doped Zr–Ce–O (Ce/Zr=1) solid solutions appear near 470 cm^{-1}.[35] It was concluded that Si dopant hardly changes the phase of the solid solution. As shown in Fig. 3(e), the relative intensities of 1057 cm^{-1} ($BaCO_3$) and 466 cm^{-1} $[(Zr,Ce,Y)O_2]$ increase significantly after exposure to CO_2, but the intensity of 356 cm^{-1} vibration decreases.

Figure 4(a) shows the XRD spectrum of BZCY532 powder before exposure to CO_2. The cubic lattice parameter was estimated to be a=4.307 Å. Some minor shoulders (or splittings) as indicated by * are possibly caused by a slight rhombohedral distortion from the cubic structure because $BaZr_{1-x}Ce_xO_3$ is possibly rhombohedral for $0.15<x<0.5$.[31] In that work, the composition we would call BZCY640 (no Y) was rhombohedral below and cubic above 477 °C. Regarding the effect of adding 0.2 fraction Y to replace 0.1 each of Zr and Ce, the closest comparison available is adding 0.1 Y to $BaCeO_3$. This changes the $Pnma/Imma/R\bar{3}c/c/Pm\bar{3}m$ transition temperatures from 290/400/900 to 237/462/767 °C.[30] These small but significant changes indicate that a small part of the BZCY532 sample could have been in rhombohedral phase over observed temperature range. This type of perovskite can crystallize in various phases, depending on processing method and sintering temperature. For example, Melekh *et al.*[36] reported that different workers found orthorhombic, cubic, pseudocubic, and tetragonal phases at room temperature for $BaCeO_3$ prepared by various methods.

The XRD spectra of BZCY532 powder remain un-

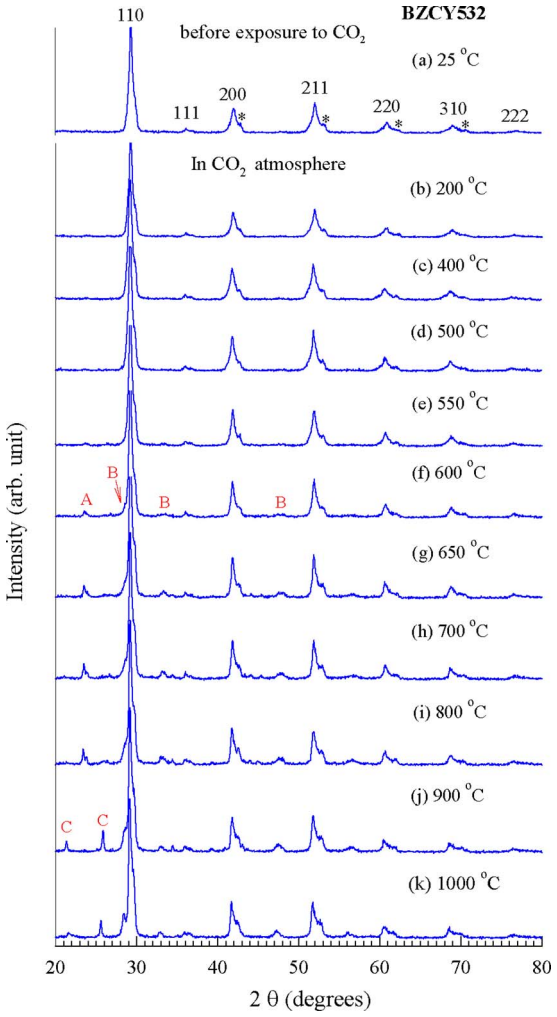

FIG. 4. (Color online) Temperature-dependent XRD spectra of BZCY532.

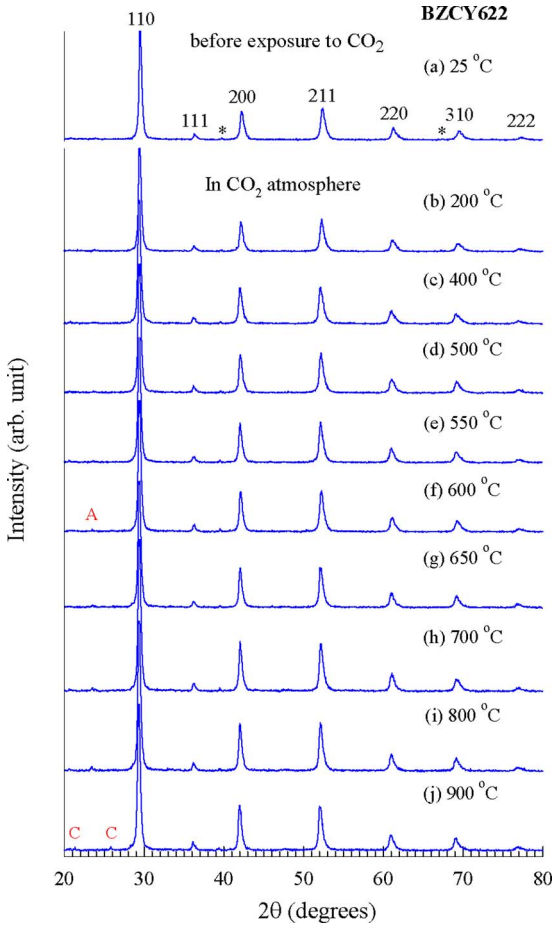

FIG. 5. (Color online) Temperature-dependent XRD spectra of BZCY622.

changed below 550 °C (Fig. 4). $BaCO_3$ and $(Zr,Ce,Y)O_2$ structures appear noticeably at 550 and 600 °C as indicated by A and B, respectively. They increase in amplitude with temperature and the A peak splits above 800 °C because of the orthorhombic-hexagonal transition of $BaCO_3$. As shown in Fig. 3(f), the decomposition of BZCY532 was confirmed by the 470 cm^{-1} vibration of $(Zr,Ce,Y)O_2$ and 689, 1057, and 1417 cm^{-1} vibrations of $BaCO_3$. It was found that BZCY532 can absorb about 0.03 g of CO_2 per ceramic gram after exposure to CO_2 from 900 °C.

The XRD spectrum of BZCY622 powder before exposure to CO_2 is given in Fig. 5(a). The cubic lattice parameter was estimated to be $a=4.279$ Å. Two very weak peaks as indicated by * near the (200) and (310) peaks correlate to a second phase. As shown in Fig. 5, BZCY622 remains thermally stable in CO_2 up to 900 °C with a very slight decomposition above 550 K [Figs. 5(f)–5(j)]. This stability is confirmed by the Raman spectra [Fig. 3(g)], in which there is no much difference before and after exposure to CO_2. The weak 1057 cm^{-1} vibration before exposure to CO_2 indicates a very small amount of $BaCO_3$ likely formed in the calcining process.

The Raman spectra of BZCY442, BZCY532, and BZCY622 powders before exposure to CO_2 [Figs. 3(e)–3(g)] show that the 356 (or 357 cm^{-1}) vibrations and its shoulder (about 370 cm^{-1}) become weaker as cerium content decreases, indicating that the 356 (or 357) and 370 cm^{-1} vibrations are sensitive to cerium content. These are consistent with the Raman result of $BaZr_{1-x}Ce_xO_3$,[31] in which the relative intensities of these vibrations (356 and 370 cm^{-1}) decrease and their frequencies also shift to higher region as x decreases.

Just as for BZCY622, BZY82 powder demonstrates a good thermal stability in CO_2 as evidenced in Figs. 6 and 3(h). Some weak peaks of Y_2O_3-like structure were observed as indicated by "D," which was confirmed by the Raman vibration of 374 cm^{-1} [Figs. 3(c) and 3(h)]. The cubic lattice parameter of BZY82 is $a=4.216$ Å. This is slightly larger than the lattice constant $a=4.192$ Å of cubic $BaZrO_3$ (Ref. 31) because the ionic radius of Y^{3+} ($R^{III}=0.9$ Å) is larger than for Zr^{4+} ($R^{IV}=0.72$ Å). The lattice parameters of BZY82 (4.216 Å), BZCY622 (4.279 Å), BZCY532 (4.307 Å), and BZCY442 (4.322 Å) increase with Ce content because the radius of Ce^{4+} ($R^{IV}=0.87$ Å) is larger than for Zr^{4+} ($R^{IV}=0.72$ Å).[37] Figure 7 shows a nearly linear relation between lattice parameter and Zr content.

As shown in the results and discussion described above, no apparent decompositions of $BaCO_3$ and $(Zr,Ce,Y)O_2$ were detected below 550 °C, and the BZCY622 and BZY82 exhibit significant thermal stability in CO_2 at intermediate temperatures (600–900 °C). To clarify the kinetic stability

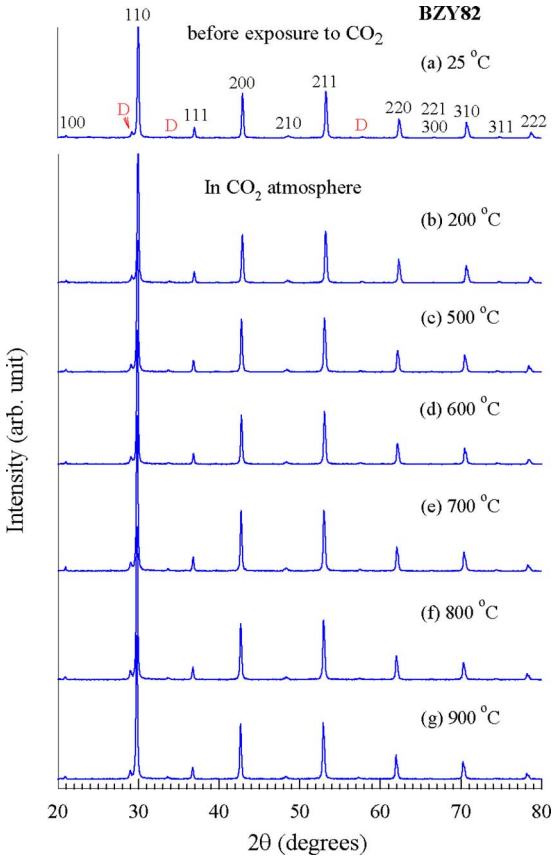

FIG. 6. (Color online) Temperature-dependent XRD spectra of BZY82. D indicates the Y_2O_3-like structure.

below and above 550 °C, time-dependent XRD spectra in CO_2 were measured at 500 and 700 °C separately, as shown in Fig. 8. The term kinetic stability describes a metastable chemical state that is trapped because of a high activation energy barrier, which causes a very slow reaction rate or essentially none at all, to reach the stable state.

After a long duration (about 29 h) in 1 atm CO_2 at 500 °C [Fig. 8(a)], no apparent decomposition was detected in BZCY442 and BZCY532, indicating a kinetic stability below 500 °C. However, at 700 °C [Fig. 8(b)] both BZCY442 and BZCY532 showed an obvious chemical decomposition as indicated by A and B peaks, which grows as the exposure time increases. Note that both orthorhombic

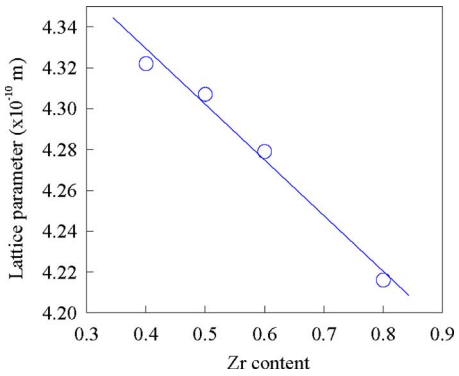

FIG. 7. (Color online) Lattice parameter vs Zr content before exposure to CO_2.

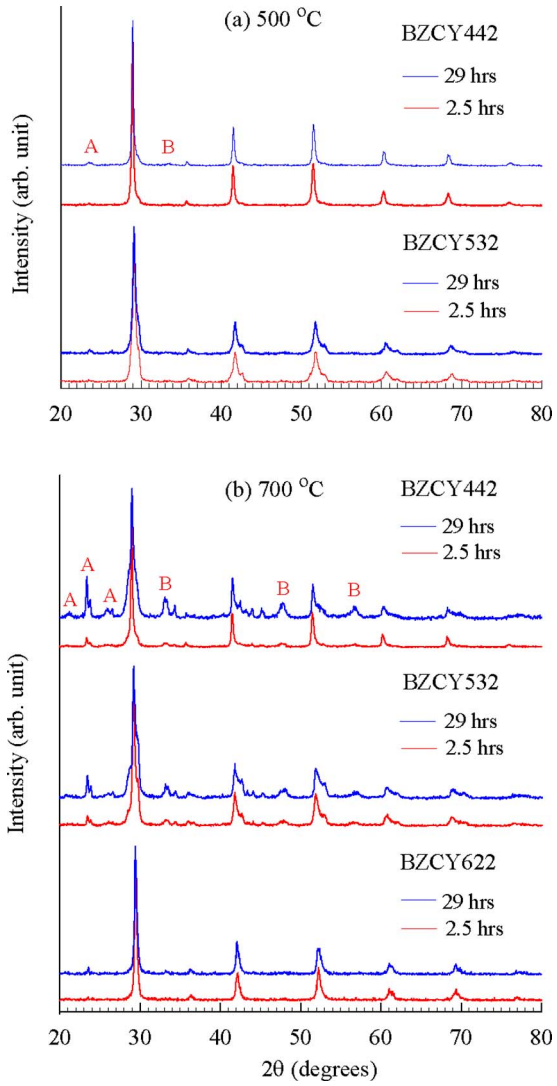

FIG. 8. (Color online) Time-dependent XRD spectra in CO_2 at 500 and 700 °C. A and B correspond to orthorhombic and hexagonal $BaCO_3$ and cubic $(Zr,Ce,Y)O_2$, respectively.

and hexagonal structures of $BaCO_3$ appear after a long duration at 700 °C, indicating that the orthorhombic-hexagonal structural transformation could occur at lower temperature if the exposure time in CO_2 is longer enough. The time-dependent relative intensity between the A peak ($2\theta \cong 24°$) of $BaCO_3$ and the (110) peak ($2\theta \cong 29°$) is plotted in Fig. 9. The relative intensity of $BaCO_3$ at 700 °C grows obviously as exposure time increases in both BZCY442 and BZCY532, especially for BZCY442 which exhibits a rapid decomposition of $BaCO_3$ and $(Zr,Ce,Y)O_2$. Compared with BZCY442 and BZCY532, BZCY622 demonstrates a much better kinetic stability at 700 °C. The kinetic instability of BZCY442 and BZCY532 at 700 °C was also confirmed by the post-Raman spectra, as shown in Figs. 10(a) and 10(b), respectively. As seen in Fig. 10(c), no apparent decomposition was detected in BZCY622 after a long duration in CO_2 at 700 °C.

As shown in Fig. 9, both BZCY442 and BZCY532 exhibit similar slopes of relative intensity versus exposure time at 700 °C below 13 h. In BZCY442, $BaCO_3$ concentration rises almost linearly with exposure time with an extrapolated

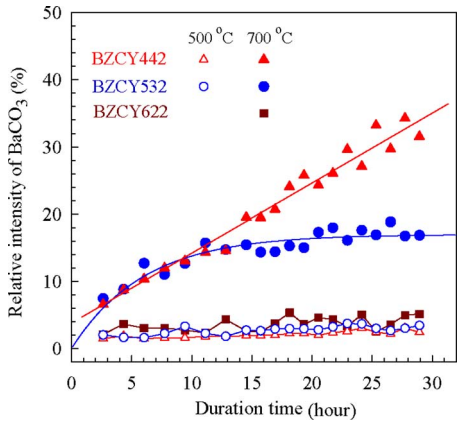

FIG. 9. (Color online) Time-dependent relative intensity between the $BaCO_3$ peak ($2\theta \cong 24°$) and (110) peak at 500 and 700 °C. The solid blue curve is the fitting of the exponential rise equation for BZCY532 at 700 °C.

zero-time intercept of 4%. For BZCY532, the time-dependent relative intensity at 700 °C can be approximately described by the exponential rise equation $n(t)=n_S[1-e^{-t/\tau}]$ with $n_S=17\%$ and $\tau=6$ h as indicated by the solid curve. $n(t)$ is the time-dependent $BaCO_3$ concentration and τ is the rise time constant. The saturation concentration of $n_S=17\%$ implies that the carbonate forms a protective layer that keeps CO_2 from reacting with the interior of the powders.

IV. CONCLUSIONS

$Ba(Zr_{0.8-x}Ce_xY_{0.2})O_{2.9}$ ($x=0.0$, 0.2, 0.3, and 0.4) ceramics exhibit a promising thermal stability below 550 °C without apparent chemical decomposition in 1 atm CO_2. As temperature rises, the low-cerium compounds $Ba(Zr_{0.8-x}Ce_xY_{0.2})O_{2.9}$ ($x \leq 0.2$) retain kinetic stability up to 1000 °C after a long-duration exposure to CO_2. An orthorhombic-hexagonal structure transformation of $BaCO_3$ was evidenced in the region of 810–850 °C in BZCY442 and BZCY532 upon heating. Raman vibrations of 1057 and 466 cm^{-1} exhibit high sensitivity to appearances of $BaCO_3$ and $(Zr,Ce,Y)O_2$, respectively. Both XRD spectra and Raman vibrations of ZrO_2, CeO_2, and Y_2O_3 powders were also obtained at room temperature and can be useful for identification of these compounds. This study suggests that $Ba(Zr_{0.8-x}Ce_xY_{0.2})O_{2.9}$ ceramics with $x \leq 0.2$ are promising candidates for proton-conducting SOFC applications at intermediate temperatures (700–850 °C).

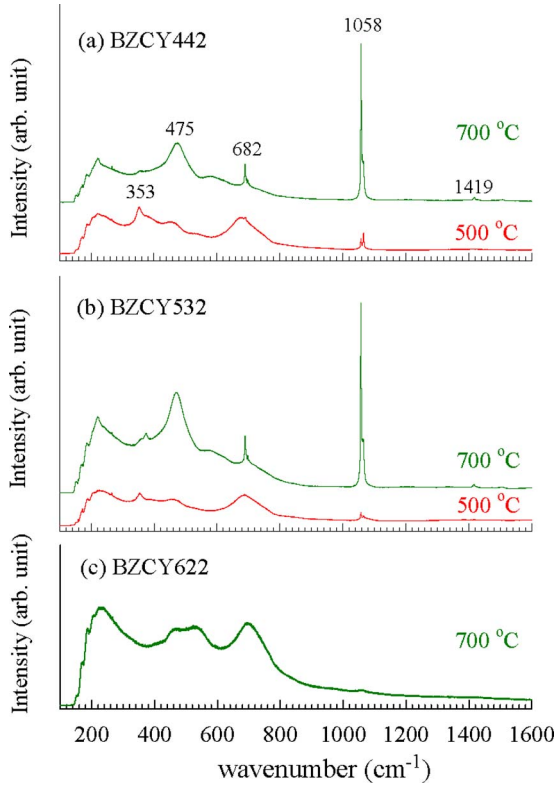

FIG. 10. (Color online) Post-Raman spectra of (a) BZCY442, (b) BZCY532, and (c) BZCY622 powders after long-duration exposures in CO_2 at 500 and 700 °C.

The authors would like to thank Dr. J. Liang (Fu Jen Catholic University) for the Raman scattering apparatus. This work was supported by National Science Council of Taiwan (Grant No. 96-2112-M-030-001) and DOE under subcontract DE-AC06-76RL01830 from Battelle Memorial Institute and Pacific Northwest National Laboratory.

[1] J. P. Trembly, R. S. Gemmen, and D. J. Bayless, J. Power Sources **163**, 986 (2007).
[2] R. S. Gemmen and J. P. Trembly, J. Power Sources **161**, 1084 (2006).
[3] M. Gong, X. Liu, J. P. Trembly, and C. Johnson, J. Power Sources **168**, 289 (2007).
[4] S. McIntosh and R. J. Gorte, Chem. Rev. (Washington, D.C.) **104**, 4845 (2004).
[5] S. M. Haile, Acta Mater. **51**, 5981 (2003).
[6] C. W. Tanner and A. V. Virkar, J. Electrochem. Soc. **143**, 1386 (1996).
[7] S. V. Bhide and A. V. Virkar, J. Electrochem. Soc. **146**, 2038 (1999).
[8] N. Zakowsky, S. Williamson, and J. T. S. Irvine, Solid State Ionics **176**, 3019 (2005).
[9] B. R. Sneha and V. Thangadurai, J. Solid State Chem. **180**, 2661 (2007).
[10] F. Chen, O. T. Sorensen, G. Meng, and D. Peng, J. Mater. Chem. **7**, 481 (1997).
[11] G. Ma, T. Shimura, and H. Iwahara, Solid State Ionics **110**, 103 (1998).
[12] K. Katahira, Y. Kohchi, T. Shimura, and H. Iwahara, Solid State Ionics **138**, 91 (2000).
[13] Z. Zhong, Solid State Ionics **178**, 213 (2007).
[14] F. M. M. Snijkers, A. Buekenhoudt, J. Cooymans, and J. J. Luyten, Scr. Mater. **50**, 655 (2004).
[15] A. Magrez and T. Schober, Solid State Ionics **175**, 585 (2004).
[16] K. H. Ryu and S. M. Haile, Solid State Ionics **125**, 355 (1999).
[17] S. M. Haile, G. Staneff, and K. H. Ryu, J. Mater. Sci. **36**, 1149 (2001).
[18] C. Zuo, S. Zha, M. Liu, M. Hatano, and M. Uchiyama, Adv. Mater. (Weinheim, Ger.) **18**, 3318 (2006).
[19] A. S. Patnaik and A. V. Virkar, J. Electrochem. Soc. **153**, A1397 (2006).
[20] P. Babilo, T. Uda, and S. M. Haile, J. Mater. Res. **22**, 1322 (2007).
[21] P. Babilo and S. M. Haile, J. Am. Ceram. Soc. **88**, 2362 (2005).
[22] A. K. Azad and J. T. S. Irvine, Solid State Ionics **178**, 635 (2007).
[23] S. S. Bhella and V. Thangadurai, J. Power Sources **186**, 311 (2009).
[24] L. A. Chick, L. R. Pederson, G. D. Maupin, J. L. Bates, L. E. Thomas, and G. J. Exarhos, Mater. Lett. **10**, 6 (1990).
[25] B. D. Cullity, *Elements of X-ray Diffraction* (Addison-Wesley, Reading, MA, 1978).
[26] R. Strobel, M. Maciejewski, S. E. Pratsinis, and A. Baiker, Thermochim. Acta **445**, 23 (2006).
[27] C. R. M. Rao and P. N. Mehrotra, J. Therm. Anal. **17**, 539 (1979).
[28] M. Yoshimura, Am. Ceram. Soc. Bull. **67**, 1950 (1988).
[29] M. Yashima, D. Ishimura, Y. Yamaguchi, K. Ohoyama, and K. Kawachi, Chem. Phys. Lett. **372**, 784 (2003).
[30] K. S. Knight, Solid State Ionics **145**, 275 (2001).
[31] I. Charrier-Cougoulic, T. Pagnier, and G. Lucazeau, J. Solid State Chem. **142**, 220 (1999).
[32] B.-K. Kim and H.-O. Hamaguchi, Phys. Status Solidi B **203**, 557 (1997).
[33] R. Q. Long, Y. P. Huang, and H. L. Wan, J. Raman Spectrosc. **28**, 29

(1997).
[34]R. L. Frost and J. M. Bouzaid, J. Raman Spectrosc. **38**, 873 (2007).
[35]X. Wang, G. Lu, Y. Guo, Y. Xue, L. Jiang, Y. Guo, and Z. Zhang, Catal. Today **126**, 412 (2007).
[36]B.-T. Melekh, V. M. Egorov, Y. M. Baikov, N. F. Kartenko, Y. N. Filin, M. E. Kompan, I. I. Novak, G. B. Venus, and V. B. Kulik, Solid State Ionics **97**, 465 (1997).
[37]R. D. Shannon, Acta Crystallogr. **A32**, 751 (1976).